High-precision measurement of lifetimes and collisional decay parameters in Ca ^1D states using the two-photon Hanle effect

L. R. Hunter, G. M. Watson, D. S. Weiss, and A. G. Zajonc
Department of Physics, Amherst College, Amherst, Massachusetts 01002
(Received 26 October 1984)

We report high-precision measurements of the lifetimes and collisional decay parameters of the $(4p^2)\,^1D$ and $(4s\,5d)\,^1D$ states of atomic calcium using the two-photon Hanle effect. Modification of the excited-state decay rates due to saturation of the two-photon transition is clearly observed. Spontaneous-emission rates of the possible dipole transitions from these states are deduced through branching-ratio measurements and compared with theory. The $(4s\,4d)^1D$ lifetime is determined through observation of its exponential decay.

I. INTRODUCTION

The Hanle effect has long been established as a high-precision tool for the determination of atomic lifetimes and collisional decay parameters. Traditionally, the Hanle effect using only optical excitation has been confined to states with parity opposite to that of the atomic ground state. With the advent of pulsed lasers, however, two-photon excitation to states of the same parity as the atomic ground state is possible. If the laser light is polarized, magnetic coherences are produced in the excited state and the Hanle effect may be observed via the decay fluorescence. This technique has several features which make it particularly attractive as a high-precision experimental tool.

(1) The fluorescence wavelength is different from the excitation wavelength, permitting elimination of backgrounds from scattered laser light.

(2) There is no resonance trapping to the ground state of either the incident or decay fluorescent light, and so high densities may be used.

(3) Highly excited states may be accessed because of the two-photon excitation process.

(4) The excitation process is highly selective and nonperturbative.

Previously, the two-photon Hanle effect was used to investigate the collisional relaxation parameters of the $4D$ level of sodium.[1] Lifetimes of Tl $P_{3/2}$ states have been measured using the two-photon Hanle effect,[2] however, an error in the analysis led to an overestimation of the lifetimes by about 13%. The present work, we believe, represents the first correct lifetime determination using the two-photon Hanle effect as well as the highest-precision measurement of the collisional decay parameters of atomic D states. Ratios of these decay parameters show an interesting dependence on the species of buffer gas that has not been previously noted.

Precise lifetime measurements in the Ca D series are required to provide calibration for recent high-precision relative oscillator-strength measurements.[3] These oscillator strengths are important for the determination of the Ca abundance in solar-type stars.[4] In addition, the present results resolve a discrepancy that existed between these oscillator-strength measurements and a previously reported lifetime measurement.[5]

The Ca ^1S ground state is excited to a ^1D state by a degenerate two-photon process. We use the density-matrix formalism to analyze the two-photon Hanle effect. Only a sketch of the derivation will be presented here as other authors have already presented detailed calculations for other transitions.[6]

II. THEORY

A. Density-matrix representation of the two-photon Hanle effect

The evolution of the density matrix ρ associated with the atomic excited state is $\partial\rho/\partial t=-(i/\hbar)[H,\rho]-\Gamma\rho+(\partial\rho/\partial t)^e$, where H is the Hamiltonian associated with the applied magnetic field. The second term represents spontaneous emission while the last term represents two-photon excitation and may be expressed as

$$(\partial\rho/\partial t)^e_{mm'}=\lambda(\rho_0)_{mm'}\ ,$$

where λ is proportional to the two-photon excitation rate and independent of the magnetic sublevels m and m'. $(\rho_0)_{mm'}$ is defined by

$$(\rho_0)_{mm'}=\sum_{i,i'}\langle m\,|\,\hat{\epsilon}\cdot\hat{\mathbf{D}}\,|\,i\rangle\langle i\,|\,\hat{\epsilon}\cdot\hat{\mathbf{D}}\,|\,g\rangle \times\langle g\,|\,\hat{\epsilon}^*\cdot\hat{\mathbf{D}}\,|\,i'\rangle\langle i'\,|\,\hat{\epsilon}^*\cdot\hat{\mathbf{D}}\,|\,m'\rangle\rho_g\ ,$$

where $\hat{\epsilon}$ is the polarization of the excitation radiation and $\hat{\mathbf{D}}$ is the normalized dipole operator. The magnetic sublevels of the excited ^1D state are $|\,m\,\rangle$ and $|\,m'\,\rangle$, while $|\,i\,\rangle$ and $|\,i'\,\rangle$ are magnetic sublevels of the virtual intermediate ^1P states and $|\,g\,\rangle$ is the ^1S ground state. The ground-state density matrix is designated by ρ_g.

The geometry of our experiment is shown in Fig. 1. With the magnetic field along $\hat{\mathbf{k}}$ the Zeeman Hamiltonian is $H=\hbar\omega J_z$; where $\omega=g_J\mu_0 B/\hbar$ is the Larmor precession frequency of the excited state and J_z is the component of

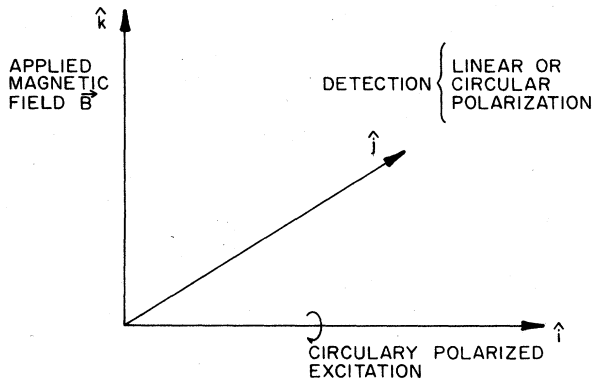

FIG. 1. Experimental geometry.

the angular momentum operator in the $\hat{\mathbf{k}}$ direction. The stationary-state solution for the excited-state density matrix is then found to be

$$(\rho_s)_{mm'}=\lambda(\rho_0)_{mm'}/[\Gamma+i(m-m')\omega] .$$

The light intensity due to dipole decay fluorescence as seen by a detector sensitive only to light with polarization $\hat{\epsilon}'$ will be proportional to

$$I=\sum_{f,m,m'}\langle f\,|\hat{\epsilon}'\cdot\hat{\mathbf{D}}\,|\,m\rangle(\rho_s)_{mm'}\langle m'\,|\hat{\epsilon}'^{*}\cdot\hat{\mathbf{D}}\,|\,f\rangle .$$

$|f\rangle$ labels the magnetic sublevel of the final atomic state which is in the present work a ^1P state. Using the above formalism one finds the following expressions for the emitted intensity. For linear polarization analysis along $\hat{\mathbf{i}}$ ($\hat{\epsilon}'=\hat{\mathbf{i}}$) we have

$$\begin{aligned}I_x=\{&[6(\rho_s)_{-2,-2}+3(\rho_s)_{-1,-1}\\&+2(\rho_s)_{00}+3(\rho_s)_{11}+6(\rho_s)_{22}]\\&-\sqrt{6}[(\rho_s)_{02}+(\rho_s)_{20}+(\rho_s)_{-2,0}+(\rho_s)_{0,-2}]\\&-3[(\rho_s)_{1,-1}+(\rho_s)_{-1,1}]\}/12 .\end{aligned}\tag{1}$$

While for linear polarization analysis along $\hat{\mathbf{k}}$ ($\hat{\epsilon}'=\hat{\mathbf{k}}$) we have

$$I_z=[3(\rho_s)_{11}+4(\rho_s)_{00}+3(\rho_s)_{-1,-1}]/6 .\tag{2}$$

If collisions are neglected these expressions, yield for the incident light linearly polarized along $\hat{\mathbf{j}}$ ($\hat{\epsilon}=\hat{\mathbf{j}}$)

$$I_x=\lambda[5-3\Gamma^2/(\Gamma^2+4\omega^2)]/18\Gamma \text{ and } I_z=\lambda/9\Gamma ,$$

while for circular polarization incident $[\hat{\epsilon}=(\hat{\mathbf{k}}\pm i\hat{\mathbf{j}})/\sqrt{2}]$ one finds

$$I_x=\lambda[1-\Gamma^2/(\Gamma^2+4\omega^2)]/4\Gamma \text{ and } I_z=\lambda/2\Gamma .$$

Notice that unlike the case of $S\rightarrow P$ excitation, I_x does not vanish when the incident polarization is along $\hat{\mathbf{j}}$ and the magnetic field is zero. It is evident from examining the above expressions that greater sensitivity will be obtained using incident circularly polarized light.

For the case of circular polarization analysis $[\hat{\epsilon}'=(\hat{\mathbf{k}}\pm i\hat{\mathbf{i}})/\sqrt{2}]$ one finds

$$\begin{aligned}I_{\pm}=&[6(\rho_s)_{22}+9(\rho_s)_{11}+10(\rho_s)_{00}+9(\rho_s)_{-1,-1}+6(\rho_s)_{-2,-2}]/24\\&-[2(\rho_s)_{02}+\sqrt{6}(\rho_s)_{-1,1}+2(\rho_s)_{-2,0}+2(\rho_s)_{20}+\sqrt{6}(\rho_s)_{1,-1}+2(\rho_s)_{0,-2}]/8\sqrt{6}\\&\pm i\{-[\sqrt{6}(\rho_s)_{21}+3(\rho_s)_{10}+3(\rho_s)_{0,-1}+\sqrt{6}(\rho_s)_{-1,-2}]+[\sqrt{6}(\rho_s)_{12}+3(\rho_s)_{01}+3(\rho_s)_{-1,0}+\sqrt{6}(\rho_s)_{-2,-1}]\}/4\sqrt{6} ,\end{aligned}\tag{3}$$

where the $\pm$ sign refers to a reversal of either the incident or the detected circular polarization. For the incident light linearly polarized along $\hat{\mathbf{j}}$ ($\hat{\epsilon}=\hat{\mathbf{j}}$)

$$I_{\pm}=\lambda[7-3\Gamma^2/(\Gamma^2+4\omega^2)]/36\Gamma ,$$

while for circular polarization incident $[\hat{\epsilon}=(\hat{\mathbf{k}}\pm i\hat{\mathbf{j}})/\sqrt{2}]$

$$I_{\pm}=\lambda[3-\Gamma^2/(\Gamma^2+4\omega^2)\pm 4\omega\Gamma/(\Gamma^2+\omega^2)]/8\Gamma .\tag{4}$$

In the above expressions the terms which change sign when the sign of ω is reversed (i.e., the dispersive terms) depend on coherences between levels where $m-m'=\pm 1$ (i.e., orientations) while the terms which go like $\Gamma^2/(\Gamma^2+4\omega^2)$ depend on coherences between levels where $m-m'=\pm 2$ (i.e., alignments). In order to be sensitive to both of these types of terms and to be able to clearly distinguish between them we have chosen to perform our experiments with the excitation radiation circularly polarized and to perform detection with both circular and linear polarization analyzers. Neglect of the second term in Eq. (4) led to the analysis error made in Ref. 2.

B. The effects of collisions

Thus far, the effects of collisions with the buffer gas have been neglected. In the presence of a buffer gas there are in principle five independent collisional parameters associated with a ^1D state, one collisional decay rate associated with each order of the irreducible tensor representation. To include the effects of collisions, the density-matrix components must be reexpressed in terms of their irreducible tensor components

$$\rho=\sum_{k=0}^{2}\sum_{q=-k}^{k}\rho_k^q T_q^k ,$$

where k is the order of the tensor and q its component. The coefficients in the expansion may be expressed as

$$\rho_k^q = \mathrm{Tr}(\rho T_q^k) = \sum_{m,m'} \rho_{mm'} \langle m' \mid T_q^k \mid m \rangle .$$

The important decompositions for the present problem are

$$\sqrt{5}\rho_0^0 = \rho_{22}+\rho_{11}+\rho_{00}+\rho_{-1,-1}+\rho_{-2,-2} ,$$
$$\sqrt{14}\rho_2^0 = 2\rho_{22}-\rho_{11}-2\rho_{00}-\rho_{-1,-1}+2\rho_{-2,-2} ,$$
$$\sqrt{14}\rho_2^2 = 2\rho_{02}+\sqrt{6}\rho_{-1,1}+2\rho_{-2,0} ,$$
$$\sqrt{14}\rho_2^{-2} = 2\rho_{20}+\sqrt{6}\rho_{1,-1}+2\rho_{0,-2} ,$$
$$\sqrt{6}\rho_1^1 = -\sqrt{2}\rho_{12}-\sqrt{3}\rho_{01}-\sqrt{3}\rho_{-1,0}-\sqrt{2}\rho_{-2,-1} ,$$
$$\sqrt{6}\rho_1^{-1} = \sqrt{2}\rho_{21}+\sqrt{3}\rho_{10}+\sqrt{3}\rho_{0,-1}+\sqrt{2}\rho_{-1,-2} .$$

Thus Eqs. (1), (2), and (3) describing various polarization intensities may be written as

$$I_x = (4\sqrt{5}\rho_0^0+\sqrt{14}\rho_2^0)/12-\sqrt{7}/3(\rho_2^2+\rho_2^{-2})/4 ,$$
$$I_z = (2\sqrt{5}\rho_0^0-\sqrt{14}\rho_2^0)/6 ,$$

and

$$I_\pm = (8\sqrt{5}\rho_0^0-\sqrt{14}\rho_2^0)/24-\sqrt{7}/3(\rho_2^2+\rho_2^{-2})/8 \pm i\sqrt{3}(\rho_1^1+\rho_1^{-1})/4 .$$

The effect of collisions is to introduce an additional decay term for each order of the density matrix

$$d\rho_k^q/dt = -G_k\rho_k^q ,$$

where G_k is independent of q and depends only on k. These decay parameters may be expressed in terms of the effective collisional cross sections

$$G_k = n\sigma_k\bar{v} , \quad (5)$$

where n is the buffer-gas density and $\bar{v}$ is the mean collisional velocity: $\bar{v}=\sqrt{8kT/\pi\mu}$ where μ is the reduced mass of the collision pair. As usual, $k=0$, 1, and 2 correspond, respectively, to the population, orientation, and alignment of the excited state. Notice that because of the single-photon detection scheme and the lack of hyperfine structure this experiment is not at all sensitive to the higher-order multipoles, $k=3$ and 4. For simplicity of notation we define

$$\Gamma_k = \Gamma + G_k , \quad (6)$$

where Γ is the spontaneous decay rate of the atom.

Each component of the irreducible tensor representation has a stationary solution

$$(\rho_s)_k^q = \lambda(\rho_0)_k^q/(\Gamma - iq\omega) ,$$

where $(\rho_0)_k^q$ is the irreducible tensor representation of the excitation process and

$$(\rho_0)_k^q = \mathrm{Tr}(\rho_0 T_q^k) .$$

For the case of incident circular polarization the above expression yields for the intensity

$$I_x = \lambda[(4/\Gamma_0-1/\Gamma_2)-3\Gamma_2/(\Gamma_2^2+4\omega^2)]/12 ,$$
$$I_z = \lambda(2/\Gamma_0+1/\Gamma_2)/6 , \quad (7)$$
$$I_\pm = \lambda[(8/\Gamma_0+1/\Gamma_2)/3-\Gamma_2/(\Gamma_2^2+4\omega^2) \pm 4\omega/(\Gamma_1^2+\omega^2)]/8 .$$

III. DESCRIPTION OF THE APPARATUS

A schematic of the apparatus is shown in Fig. 2. The calcium (typically 10^{14} cm^{-3}) is contained in a stainless-steel cross which has been previously described.[7] The buffer-gas pressure (typically 0.2—5 Torr) is measured with an MKS Baratron. The zero of the Baratron is verified approximately every five minutes during data collection in order to eliminate thermal drifts in the meter.

Excitation of the $(4s\,5d)$, $(4p)^2$, and $(4s\,4d)$ ^1D states is done using two photons at the respective wavelengths 4660, 4912, and 5362 Å (see Fig. 3). The light is generated using a flashlamp-pumped dye laser which has been previously described.[8] An 80%-reflecting output coupler is used to minimize pulse-to-pulse fluctuations in the laser and reduce the thresholds for the various dyes. The tuning is done with a three-plate birefringent filter (Spectra Physics 573-30) and a 5-mm-thick, 30%-reflecting etalon (Virgo Optics). The optimized dyes and concentrations for the relevant wavelengths are 4660 Å ($2.6\times10^{-4}M$ LD473 in C_2H_5OH), 4912 Å ($2.2\times10^{-4}M$ LD490 in two parts CH_3OH and one part H_2O), and 5362 Å ($1.6\times10^{-4}M$ Coumarin-540 in CH_3OH). Typical laser operating parameters in the present experiment are the following: pulse length, 0.5 μsec; pulse energy, 2 mJ; linewidth, 3 GHz; repetition rate, 7 Hz; and pulse-to-pulse intensity fluctuations, 15%. The emitted laser light is linearly polarized by a Glan-laser prism and then passed through a pockels cell (Cleveland Xtals Model QX1020). The appropriate quarter-wave voltage is applied to the pockels cell to circularly polarize the transmitted light. A computer-actuated relay permits reversal of this applied voltage and hence the helicity of the laser light. Imperfections in the helicity are maintained at less than 1%. The circularly polarized light is then focused by a 50-cm-focal-length lens whose position is adjusted to optimize the signal and minimize saturation effects (see Sec. V A).

The decay fluorescence from the excited ^1D state is

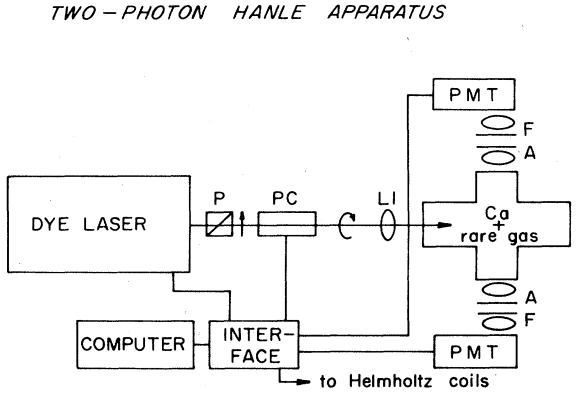

FIG. 2. Two-photon Hanle apparatus: *P*, linear polarizing prism; PC, pockels cell; *L*1, focusing lens; *A*, polarization analyzer; *F*, interference filter. The magnetic field is into the page.

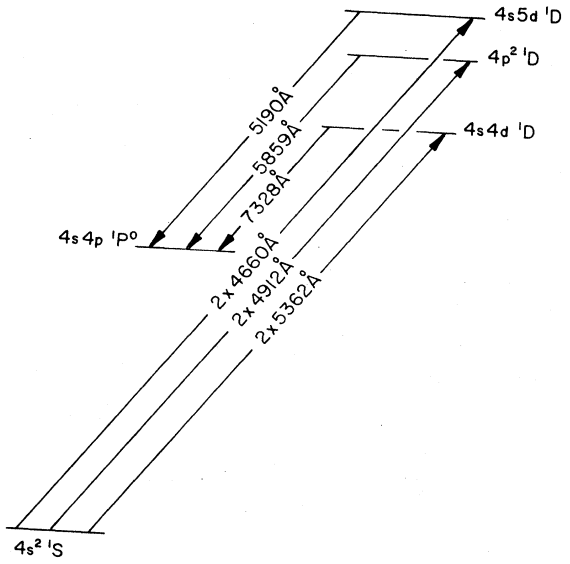

FIG. 3. Excitation and detection wavelengths for the two-photon Hanle-effect measurements (not to scale).

monitored simultaneously along the $\pm\hat{\mathbf{j}}$ directions. The fluorescence is collected and collimated by the first lens and then passed through a plastic polarization-analyzing sheet (Polaroid). For circular polarization analysis, the polarizers preceding each tube transmit the same helicity. For linear polarization analysis, one polarizer is set to transmit only light linearly polarized along $\hat{\mathbf{k}}$ ($\hat{\boldsymbol{\epsilon}}'=\hat{\mathbf{k}}$) while the opposing polarizer transmits only light linearly polarized along $\hat{\mathbf{i}}$ ($\hat{\boldsymbol{\epsilon}}'=\hat{\mathbf{i}}$). Following the plastic polarizers the fluorescence passes through bandpass filters that select the wavelength of interest [5190, 5859, and 7328 Å for the $(4s\,5d)$, $(4p^2)$, and $(4s\,4d)$ ^1D states, respectively]. Typically the bandwidth of these filters is 100 Å, however, in an effort to reduce blackbody backgrounds, 10-Å filters (Spectra Film) are used at 7328 Å. The fluorescent light is then focused down onto the photocathode of a pair of phototubes (Hamamatsu R955). The phototube output is integrated, amplified, and then digitized. The digitized signals are accumulated, analyzed, and stored by an HP 9826 computer.

The magnetic field along $\hat{\mathbf{k}}$ is created by a pair of Helmholtz coils with radii of 22 cm. Inhomogeneities of the applied field over the region of observation are thus expected to be less than 0.01%. The current for the Helmholtz pair is provided by a computer-controlled constant-current source. In addition, the sign of the applied field may be reversed by a computer-actuated relay. The magnetic field may thus be scanned over the range -30 to 30 G in 0.75-G steps. Field calibration is accomplished by using both a Hall probe (Walker Scientific) and a rotating coil gaussmeter (Rossen-Lush), both calibrated against a local NMR signal. The magnetic field calibration has a net uncertainty of approximately 0.5%. No variation of the magnetic field over the fiducial volume is observed with a sensitivity of about 0.2%.

IV. DEFINITION OF THE EXPERIMENTALLY MEASURED QUANTITIES

A. Measurements involving linear polarization analysis

Because our measurements are made using pulsed laser excitation we would like always to observe ratios of various signals on a given laser pulse so that laser intensity and frequency fluctuations will not contribute significantly to the noise. With this in mind we have chosen to construct the experimental ratio I_x/I_z, where I_x and I_z are measured on the same laser pulse. For each buffer-gas pressure we measure and plot this ratio as a function of the applied B field. In the determination of ω, g_J is assumed to be equal to 1. This approximation should be quite good for the states of interest since they do not experience strong singlet-triplet mixing. Measurements have shown that even in strontium, where the singlet-triplet mixing is expected to be much larger, deviation of g_J from 1 is insignificant except near an avoided crossing.[9] A typical experimental curve is shown in Fig. 4. Each experimental point is the average of 20 laser pulses at the indicated magnetic field, 10 pulses for each incident circular polarization. The entire scan shown represents about three minutes of data collection. These data are fit to the function

$$I_x/I_z=F\{1-C/[1-4(\omega/\Gamma_2)^2]\}\ , \tag{8}$$

where F, C, and Γ_2 are independent of ω. The resulting fit is virtually indistinguishable from the data. A plot of the fit values Γ_2 as a function of the buffer-gas pressure is shown in Fig. 5. The slope of the line determines σ_2 and the intercept Γ.

Comparing Eqs. (7) and (8) one finds that $C=3K\Gamma_0/(4\Gamma_2-\Gamma_0)$ where K is a constant that describes the overall instrumental depolarization and is independent of the buffer-gas pressure. With Γ_2 and Γ previously determined (above), the pressure dependence of C yields unique values for Γ_0 and K. This method of determining Γ_0 is unfortunately not very precise. Typically, values of K for linear polarization analysis are about 98%.

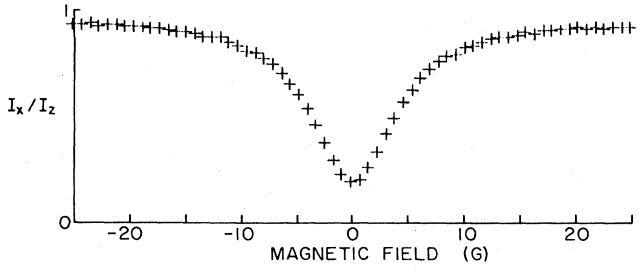

FIG. 4. Typical experimental data for linear polarization analysis. This scan is taken on the $(4p^2)\,^1D$ transition with 0.405 Torr of argon. The theoretical fit is indistinguishable from the data on this scale.

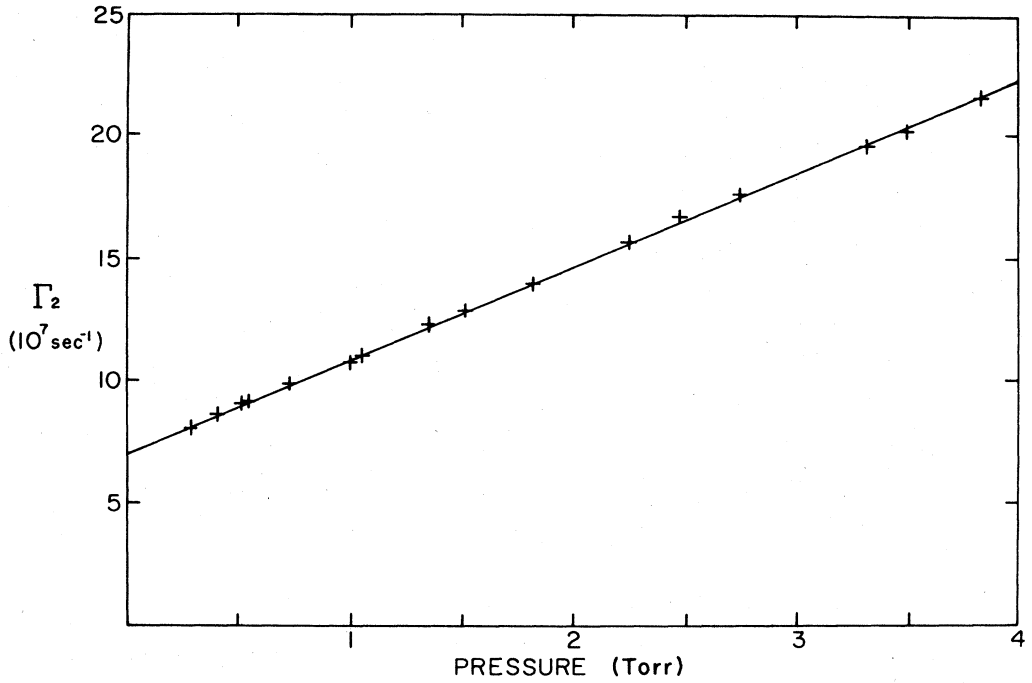

FIG. 5. The pressure dependence of the fit parameter Γ_2. The data are from the $(4p^2)\,^1D$ transition with neon as the buffer gas.

B. Measurements involving circular polarization analysis

For measurements involving circular polarization analysis of the fluorescence we construct the asymmetry $P=(I_+-I_-)/(I_++I_-)$ where I_+ and I_- are the signals on the opposing phototubes, each sensitive to the same helicity of light (and hence to opposite angular momenta). Each experimental point is again constructed from 20 laser pulses; however, the difference is now taken between asymmetries constructed with opposite incident helicities [see Eq. (7)]. A plot of a typical data scan is shown in Fig. 6. The data is fit to the function derived from Eq. (7):

$$P=\frac{4K\omega/\Gamma_1}{[1+(\omega/\Gamma_1)^2](D-(\Gamma_1/\Gamma_2)\{1/[1+4(\omega/\Gamma_2)^2]\})}, \tag{9}$$

where $D\equiv\Gamma_1(8/\Gamma_0+1/\Gamma_2)/9$ and K again represents the instrumental depolarization. The fitted curves are again practically indistinguishable from the experimental data. The width of the dispersion curve is very sensitive to the precise value of Γ_1 while the depth depends on K and D. A plot of the fit values of Γ_1 versus the buffer-gas pressure is shown in Fig. 7. The slope determines σ_1 while the intercept yields an independent measurement of Γ.

With the sensitive determination of Γ, Γ_1, and Γ_2 accomplished, the buffer-gas dependence of D yields a value for Γ_0 and hence σ_0. The total depolarization extrapolated to zero buffer-gas pressure determines K. Typically, values of K for circular polarization analysis vary between 91% and 94%.

V. RESULTS OF THE HANLE-EFFECT MEASUREMENTS

A. Lifetimes of the excited states

Data are collected for both linear and circular polarization analysis with helium, neon, argon, and krypton as buffer gases. The results for the spontaneous-decay rates Γ for the $(4p^2)^1D$ and $(4s\,5d)^1D$ states in each of the different experimental configurations are summarized in Table I. The agreement among the independent measure-

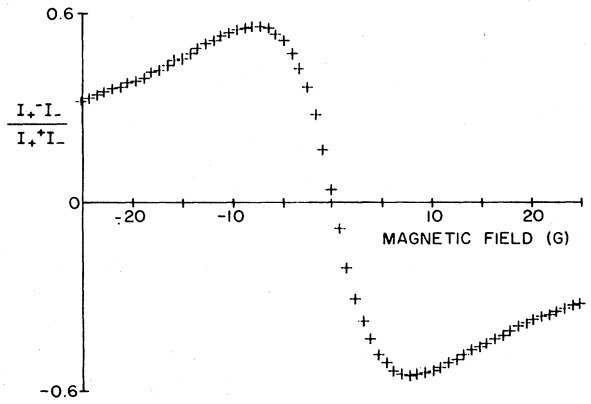

FIG. 6. Typical experimental data for circular polarization analysis. This scan is taken on the $(4p^2)\,^1D$ transition with 0.295 Torr of argon. The theoretical fit is indistinguishable from the data on this scale.

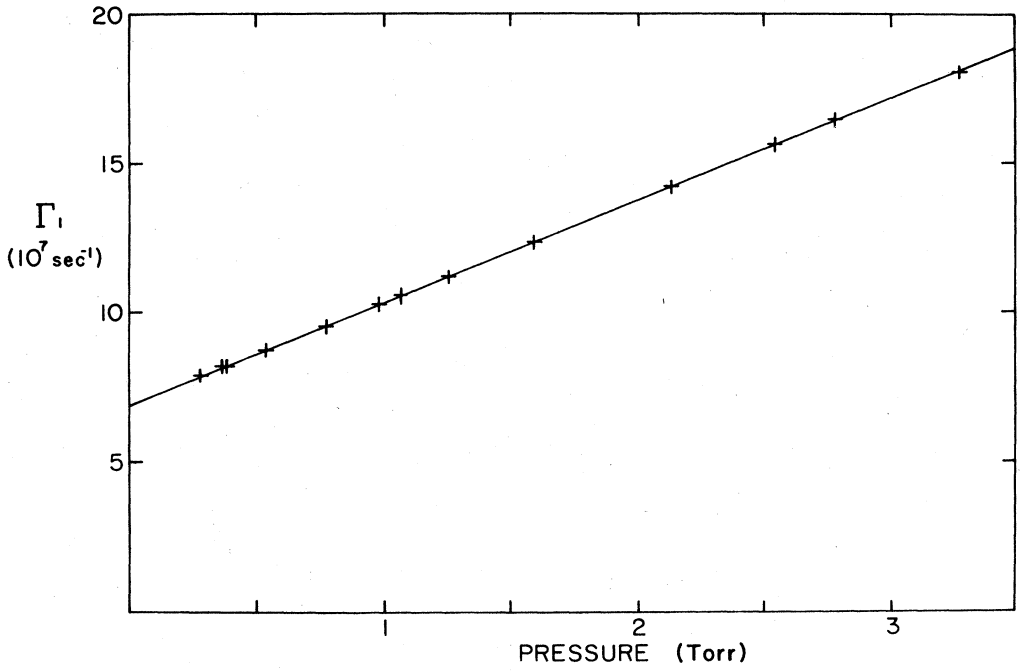

FIG. 7. The pressure dependence of the fit parameter Γ_1. The data are from the $(4p^2)\,^1D$ transition with krypton as the buffer gas.

ments is good. Systematic effects must, however, also be taken into account.

In order to study possible modification of the atomic decay rates due to the Ca-Ca collisions, the calcium density was varied by more than a factor of 4 several times during data collection. Taking into account the expected changes associated with the different mean velocities at the different cell temperatures [see Eq. (5)], no systematic changes in the decay rates are observed. The statistical uncertainties indicate that with our operating densities, Ca-Ca collisions shorten the total coherence time of the $(4p^2)^1D$ and $(4s\,5d)^1D$ states by less than 0.15% and 0.25%, respectively. This corresponds to an upper limit on the Ca-Ca collisional cross sections of about $400a_0^2$ on both transitions.

TABLE I. Measured spontaneous decay rates for the different experimental configurations. Systematics are not yet taken into account. CP, circular polarization; LP, linear polarization.

Polarization analyzed	Buffer gas	$\Gamma(4p^2\,^1D)$ (10^7 sec^{-1})	$\Gamma(4s\,5d\,^1D)$ (10^7 sec^{-1})
CP	He	6.72∓0.12	4.78∓0.06
CP	Ne	6.91∓0.03	4.72∓0.05
CP	Ar	6.95∓0.02	4.75∓0.02
CP	Kr	6.90∓0.02	4.83∓0.02
LP	He	7.07∓0.09	4.89∓0.19
LP	Ne	6.90∓0.03	4.82∓0.07
LP	Ar	6.88∓0.03	4.84∓0.05
LP	Kr	6.71∓0.06	4.71∓0.08
Weighted average		6.91∓0.02	4.79∓0.02

The effects of the laser intensity on the decay rates are easily observed and have been thoroughly studied. Through the insertion of calibrated neutral-density filters, the incident laser intensity is varied in a known manner. Hanle curves are taken and analyzed, yielding the effective decay rate at the different laser powers. The curves are found to broaden at high incident intensities. Three possible effects are considered: (1) saturation of the two-photon transition, (2) ionization of the excited state by a third photon, and (3) superfluorescence. It is found experimentally that in the region where the decay rates are not greatly modified from their asymptotic values (ie., $\Gamma_{\rm LI} \ll \Gamma$, where LI means laser induced), the modifications of the atomic decay rates are proportional to the square of the laser intensity (see Fig. 8). Process (2), which should increase linearly with the laser intensity, is thus ruled out as the dominant laser-induced decay mode for the excited state. In addition, $\Gamma_{\rm LI}$ is observed to be independent of the calcium density in this intensity regime. Process (3), which depends on the density of excited states, is thus also ruled out as the dominant effect. We conclude then that for modest laser intensities, the dominant effect of the laser intensity on the excited-state decay rate is saturation of the two-photon transition. We believe that this is the first conclusive observation of saturation in the two-photon Hanle effect.

To minimize the effect of two-photon saturation on the lifetime measurements, the laser power is *increased* and

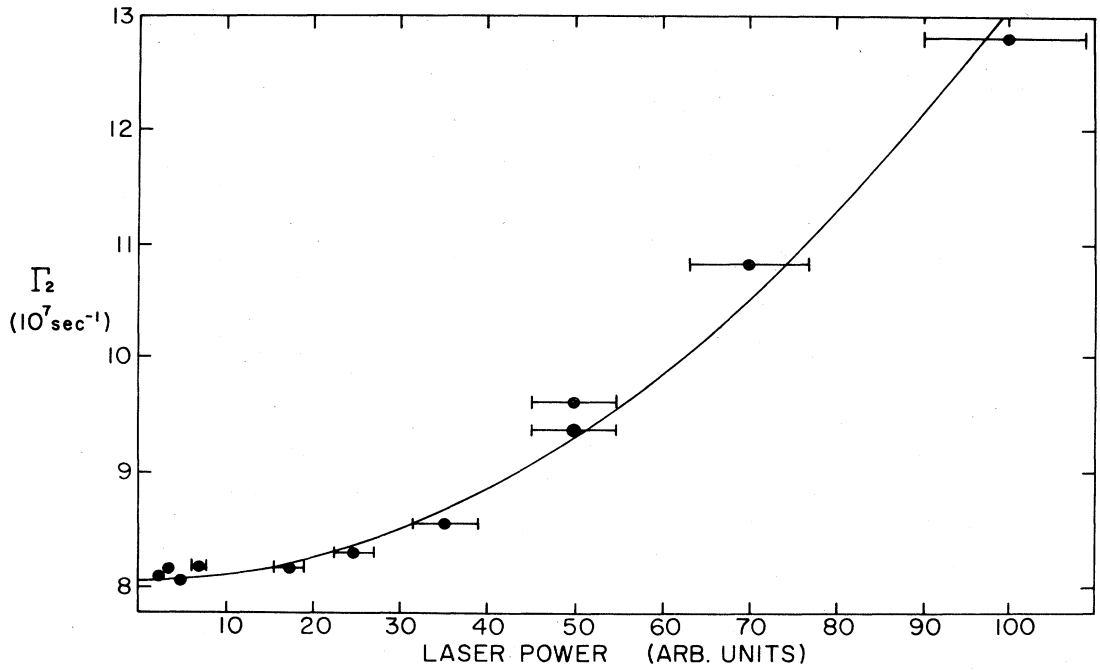

FIG. 8. The quadratic dependence of the decay rate Γ_2 on the laser power. These data were taken on the $(4p^2)\,^1D$ state with 0.28 Torr of argon. The laser is much more tightly focused than when Hanle data is taken. A 10% uncertainty in the laser power is shown for all points. The best-fit quadratic dependence is also displayed.

the beam in the cell is defocused by moving the lens $L1$. The net effect is to decrease the probability of transition per atom to an acceptable level while increasing the number of atoms illuminated so that the total signal remains adequate for detection. In this manner the effect of the laser intensity on the decay is made completely negligible for the $(4p^2)\,^1D$ state and reduced to approximately 2% for the $(4s\,5d)\,^1D$ state. A correction of $(2\pm2)\%$ is applied to take this slight saturation into account.

At much higher laser intensities the observed intensity ratios deviate substantially from the theoretical curves [Eqs. (8) and (9)] and further analysis in terms of modification of the fitting parameters is meaningless. At very high laser intensities, clear evidence of ionization is observed. This will be discussed in Sec. VII.

Being conservative and combining linearly the statistical uncertainties with the various systematic uncertainties, the following values for the lifetimes are obtained:

$$\tau(4p^2\,^1D)=14.47\pm0.14 \text{ nsec},$$

$$\tau(4s\,5d\,^1D)=21.3\pm0.7 \text{ nsec}.$$

Measurement of the $(4s\,4d)\,^1D$ lifetime is far more difficult than those already considered. The intensity of the blackbody background at 730 nm is approximately 100 times larger than at the fluorescence wavelengths of the other ^1D states. Furthermore, assuming that the $(4s\,4p)\,^1P$ state is the dominant intermediate state in the two-photon excitation, the transition rate to the $(4s\,4d)^1D$ state is only about 30% of that to the $(4p^2)^1D$ state for equal incident intensities. Even with careful spatial filtering, narrow-bandwidth interference filters, and ac coupling of the signals, higher incident light intensity (i.e., a tighter focus of the lens $L1$) is required to order to have adequate signal to noise.

The longer lifetime of the $(4s\,4d)\,^1D$ state also creates experimental difficulties. The excited state has 3 or 4 times longer to interact either with other atoms or the radiation field. Stray magnetic fields take on increased importance due to the reduced size of the applied fields.

A third important difference is the higher expected ionization rate of the $4D$ state due to the closer proximity of single-photon excitation to the ionization limit. It should be recalled that if photoionization does occur, the ionizing photon is circularly polarized and might have a profound effect on the excited state's alignment. This would show up in measurements where circular polarization is analyzed.

Despite these difficulties, Hanle curves that are nearly independent of the laser power are obtained. The lifetimes obtained from these curves for linear polarization (LP) and circular polarization (CP) detection are

$$\tau_{\mathrm{LP}}(4s\,4d\,^1D)=(59\pm4\pm2) \text{ nsec},$$

$$\tau_{\mathrm{CP}}(4s\,4d\,^1D)=(44\pm2\pm3) \text{ nsec},$$

where the first uncertainty is statistical and the second is an estimation of the laser-intensity-dependent effects. The discrepancy between these results is not yet completely understood. Such a discrepancy is not observed on either of the other ^1D states. We observe that on this transition the data involving circular polarization analysis is

TABLE II. Relaxation cross sections for the $(4p^2)\,^1D$ and $(4s\,5d)\,^1D$ states in units of $100a_0^2$. An overall normalization uncertainty of about 3% due to the temperature and magnetic field calibrations is not included.

		He	Ne	Ar	Kr
σ_0	$(4p^2)\,^1D$	0.73∓0.11	0.49∓0.08	0.79∓0.09	1.12∓0.14
σ_1	$(4p^2)\,^1D$	13.33∓0.36	11.14∓0.09	10.58∓0.08	13.36∓0.05
σ_2	$(4p^2)\,^1D$	12.31∓0.25	10.46∓0.06	10.43∓0.08	16.49∓0.22
σ_0	$(4s\,5d)\,^1D$	0.32∓0.09	0.02∓0.17	0.48∓0.21	0.30∓0.21
σ_1	$(4s\,5d)\,^1D$	25.20∓0.23	22.63∓0.24	23.58∓0.14	42.09∓0.14
σ_2	$(4s\,5d)\,^1D$	22.51∓0.69	19.56∓0.39	26.34∓0.30	50.05∓0.77

more susceptible to laser-intensity-dependent effects. Such effects, however, appear inadequate to explain the observed difference. For these reasons, we have chosen to measure this lifetime by an independent technique (see Sec. VI).

B. Collisional decay parameters for the excited states

Using the methods outlined in Sec. IV the collisional cross sections of the various states are obtained. The results are summarized in Table II. The quoted uncertainties are purely statistical. The values for σ_0 are a weighted average of the values obtained from the methods outlined in Secs. IV A and IV B. The mechanism primarily responsible for σ_0 is collisionally induced population transfer to neighboring odd-parity states. The transfer of the $(4p^2)\,^1D$ to the $(3d\,4p)\,^1F^o$ is particularly strong and has been observed through the fluorescence of the $^1F^o$ at 5350 Å.

Due to the possibility that the cell temperature might be slightly less than the thermocouple reading, the true cross sections might be higher than the values listed here by a few percent. This normalization factor is eliminated when the ratio σ_1/σ_2 is formed. For a P state this ratio was predicted[10] and observed[6] to have the value ~ 1.1, independent of the mass of the collision partner. In Table III we have calculated this ratio for each buffer gas. Also listed is a previous measurement of this ratio in the $4D$ levels of Na.[1] A decrease of the ratio as a function of increasing mass of the buffer gas is evidenced in all three transitions. We would like to suggest that if such a dependence is a general property of D states, it should be possible to predict this dependence with a theory similar to that of Ref. 10.

VI. MEASUREMENT OF THE $(4s\,4d)\,^1D$ LIFETIME BY OBSERVATION OF THE EXPONENTIAL DECAY.

Because of the discrepancy between $\tau_{\rm LP}$ and $\tau_{\rm CP}$ (Sec. V A) an independent measurement of the $(4s\,4d)\,^1D$ lifetime is required. We have chosen to measure this lifetime through observation of the exponential decay of the fluorescence after excitation by a short pulse. The two-photon transition to the $(4s\,4d)\,^1D$ state is excited using a nitrogen-pumped dye laser, previously described.[7] By examining the exponential decay fluorescence well after the 5-nsec laser pulse, laser-intensity-dependent effects are eliminated. The apparatus is only slightly modified from that described in Sec. III. The polarizing plastics are removed. The 730-nm fluorescence signal from one phototube is amplified by a fast video amplifier (Pacific 2A50) and displayed on an oscilloscope (Tektronix 7904). Two observers record the times of occurrence of a specific intensity I_0 and the intensity $I_0/3$ in the decaying exponential region of the fluorescence. From the difference of these times, the exponential decay time is deduced. Measurements of the decay times are performed at several buffer-gas pressures. The instrumental response is observed by shortening the atomic decay time below the instrumental resolution by using a very high buffer-gas pressure (~ 100 Torr Ar). The response function is adequately approximated as a decaying exponential with a characteristic decay rate $\Gamma_I = 6\times 10^7$ sec^{-1}. Sufficiently long after the laser pulse, the observed intensity profile associated with an atomic decay rate $\Gamma_A = 1/\tau_A$ may be approximated as

$$I(t) = \int_0^t e^{-\Gamma_A t'} e^{-\Gamma_I (t-t')}\,dt' = (e^{-\Gamma_A t} - e^{-\Gamma_I t})/(\Gamma_I - \Gamma_A)\,.$$

Measurements of the characteristic decay times are made at low buffer-gas pressures where $e^{-\Gamma_A t} \gg e^{-\Gamma_I t}$. The data, corrected for the detector response, are displayed in Fig. 9. The corrections varied from 2% to 8% from the lowest to the highest buffer-gas pressures shown. The intercept yields the atomic lifetime

$$\tau(4s\,4d,{}^1D) = 63 \pm 10 \text{ nsec}\,,$$

TABLE III. The ratio σ_1/σ_2 for several different buffer gases. The results for this ratio on the Na $4D$ line from Ref. 1 are also included.

		He	Ne	Ar	Kr
Ca	$(4p^2)\,^1D$	1.083∓0.051	1.065∓0.015	1.014∓0.015	0.810∓0.014
Ca	$(4s\,5d)\,^1D$	1.120∓0.045	1.157∓0.035	0.895∓0.016	0.841∓0.016
Na	4D	1.29 ∓0.27	1.26 ∓0.38	0.84 ∓0.24	0.89 ∓0.20

TABLE IV. Comparison of lifetimes τ (nsec) for levels of Ca I.

Level	a	b	c	d	e
$4s4d\ ^1D$					63 ∓10
$4p^2\ ^1D$	14.8∓1.5	17∓1.5	14.9∓0.9	17.2∓0.6	14.47∓0.14
$4s5d\ ^1D$	28 ∓3			25.2∓0.08	21.3 ∓0.7

[a]Reference 11 (e^- gun).
[b]Reference 11 (rf discharge).
[c]Reference 12.
[d]Reference 5.
[e]Present results.

where the uncertainty is approximately half due to measurement uncertainties and half due to the instrumental deconvolution. This value agrees very well with τ_{LP} but is discrepant with τ_{CP}. Because the laser pulse is already over during these measurements, this again suggests that τ_{CP} has been reduced by some light-dependent effect. Conservatively, we quote the result of this independent measurement for the $(4s4d)\ ^1D$ lifetime. To the best of our knowledge, this lifetime has not been previously reported. A summary and comparison of our lifetime measurements to previous work is shown in Table IV. The agreement is generally good. Our results support the suggestion made in Ref. 3 that the uncertainties have been underestimated in the delayed coincidence measurements of Ref. 5.

The quenching cross section of the Ca $(4s4d)\ ^1D$ state due to collisions with argon can be deduced from the slope of the line in Fig. 9. One finds

$$\sigma_0(4s4d\ ^1D \text{ on Ar}) = (30 \pm 11)a_0^2 ,$$

where the uncertainty here is about $\frac{2}{3}$ statistical, the remainder being due to the deconvolution.

VII. BRANCHING-RATIO MEASUREMENTS

In order to interpret our lifetime measurements in terms of the spontaneous decay rates to the lower levels, the branching ratios of the various decay modes are measured. Except for a few small changes, the basic apparatus for performing these measurements is the same as that described in Sec. III. The detection polarizers have been removed. One phototube continuously monitors the principal decay mode to the $(4s4p)\ ^1P$ state to provide normalization. The second phototube, now equipped with a filter holder that allows one to rapidly change interference filters, monitors alternately the principal decay mode with a fixed attenuation and one of the weak decay branches. Because the direct fluorescence to the $(4s5p)\ ^1P^o$ and $(3d4p)\ ^1D^o$ states are far into the infrared, these decays are analyzed through their subsequent decay to the $(4s3d)\ ^1D$ state at 6719 and 7150 Å, respectively (see Fig. 10). The 2722-Å fluorescence to the ground state from $(4s5p)\ ^1P^o$ is also observed. Typically, 100 laser pulses are integrated between exchanges of the detection filters. The ratio R of the weak to the principal fluorescence is formed and studied as a function of laser intensity, calcium density, and buffer-gas pressure. Several interesting effects are observed.

Under the conditions of observation, fluorescence at 2722 Å never exceeds four percent of the 6719-Å fluorescence and is neglected throughout the following discussion. This implies that the 2722-Å fluorescence is either very weak or resonantly trapped.

The fluorescence ratio R is found to increase slightly with increasing buffer-gas pressure. This effect is believed to be due to collisionally induced population transfer from the excited ^1D states to the $(4s5p)\ ^1P^o$ and

TABLE V. Transition rates in units of 10^6 sec^{-1}.

	Experiment			Theory	
Transition	a	b	c	d	e
$4s4d\ ^1D-4s4p\ ^1P$			15.9 ∓2.5	7.2	17.1
$4p^2\ ^1D-4s4p\ ^1P$	66∓10	67.6∓3.7	68.3 ∓1.1	76	55
$4p^2\ ^1D-4s5p\ ^1P$			0.7 ∓0.4		0.000
$4p^2\ ^1D-3d4p\ ^1D$			0.15∓0.07		0.40
$4s5d\ ^1D-4s4p\ ^1P$	40∓8	38.0∓1.9	46.2 ∓2.1		49
$4s5d\ ^1D-4s5p\ ^1P$			0.7 ∓0.4		0.20
$4s5d\ ^1D-3d4p\ ^1D$			<0.15		0.076

[a]Reference 13.
[b]Reference 3.
[c]Present results.
[d]Reference 14.
[e]Reference 15.

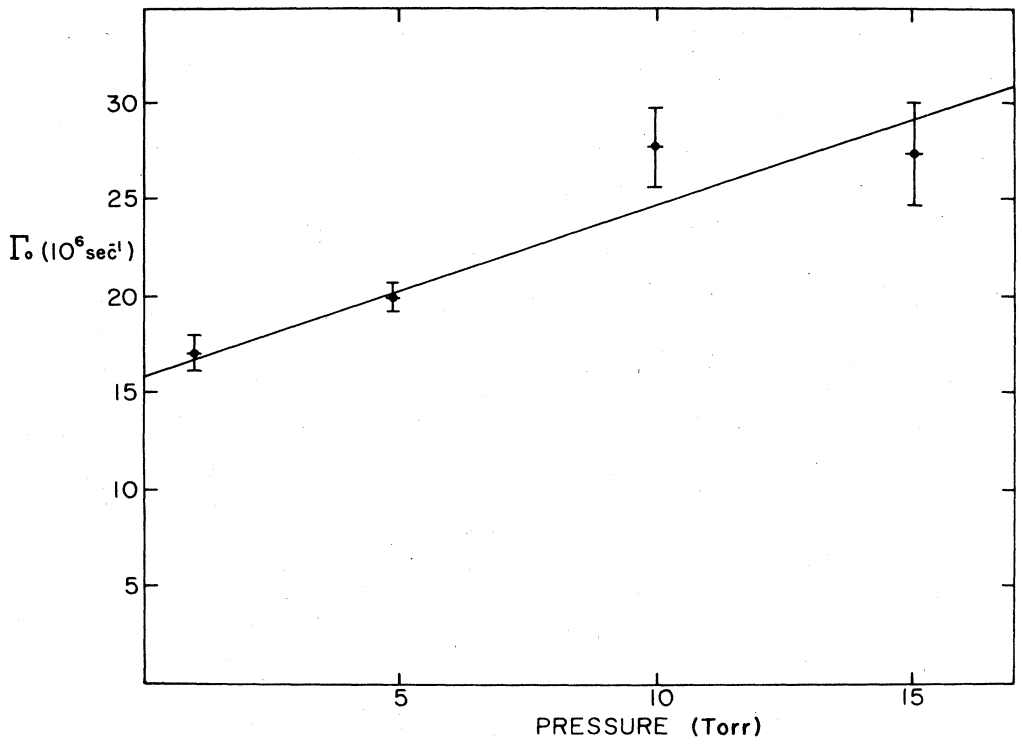

FIG. 9. Observed population decay rate of the $(4s\,4d)\,^1D$ state as a function of argon pressure. Γ_0 is obtained from measurements of the exponential fluorescence decay.

$(3d\,4p)\,^1D^o$ states. Determination of the atomic branching ratio requires extrapolation of the buffer-gas pressure to zero.

In order to measure the weak decay branches, a larger signal than that used in the Hanle effect is required. This is accomplished by slightly improving the focus of the laser beam in the cell by moving the lens $L1$. At very high laser intensities the fluorescence ratio R is found to increase rapidly with laser power. This is likely to be due to ionization of the excited state. Recombination and/or subsequent electronic excitation then produce fluorescence at virtually all of the atomic transition wavelengths, greatly enhancing the weak branches. Because these effects depend at least on the third power of the laser intensity they are easily quantified. Fortunately, it is possible to operate at intensities where these processes are unimportant.

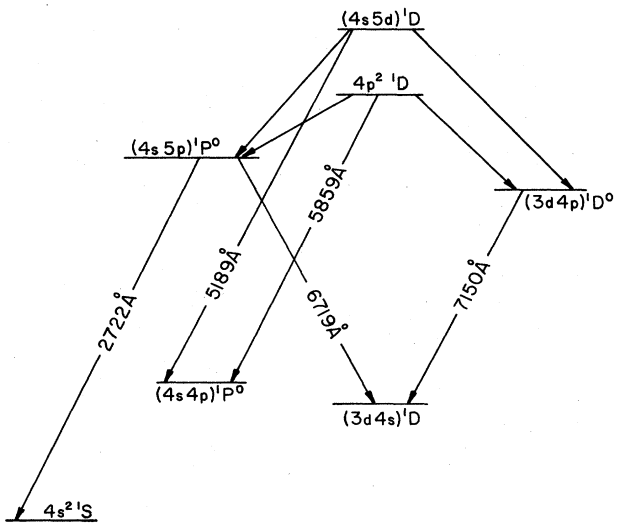

FIG. 10. The transitions observed in the branching-ratio measurements (not to scale).

Taking into account detector efficiency and filter transmission, the measured signal ratios yield the atomic branching ratios. Uncertainties in the branching-ratio measurements are dominated by systematics associated with extrapolation error, filter transmission, and the detector response.

VIII. SUMMARY AND COMPARISON OF RESULTS

The branching ratios, combined with the measured lifetimes, yield the spontaneous decay rates. These rates are summarized and compared with previous experiments and theory in Table V. The agreement is generally good. In view of the excellent agreement and high precision of the

measurements on the $(4p^2)\,^1D$-$(4s\,4p)\,^1P$ transition, this transition should now provide a reliable calibration for future relative oscillator-strength measurements in calcium. A high degree of cancellation between different configurational mixtures yields a very small theoretical result for the $(4p^2)\,^1D$-$(4s\,5p)\,^1P$ transition.[15] This is not consistent with our observation.

ACKNOWLEDGMENTS

We thank E. D. Commins and W. L. Lichten for important equipment loans. This research was supported by a grant from Research Corporation. Acknowledgment is also made to Amherst College for the special research funds made available for this project.

[1]F. Biraben, K. Beroff, G. Grynberg, and E. Giacobino, J. Phys. (Paris) **40**, 519 (1979).
[2]L. Hunter, E. Commins, and L. Roesch, Phys. Rev. A **25**, 885 (1982).
[3]G. Smith and D. St. J. Raggett, J. Phys. B **14**, 4015 (1981).
[4]H. Holweger, Solar Phys. **25**, 14 (1972).
[5]A. L. Osherovich and S. A. Pul'kin, Vestn. Leningr. Univ., Fiz., Khim. **16**, 58 (1977).
[6]J. P. Barrat, D. Casalta, J. L. Cojan, and J. Hamel, J. Phys. (Paris) **27**, 608 (1966).
[7]A. Zajonc, Phys. Rev. A **25**, 2830 (1982).
[8]S. Chu and R. W. Smith, Opt. Commun. **28**, 221 (1979).
[9]J. J. Wynne, J. A. Armstrong, and P. Esherick, Phys. Rev. Lett. **39**, 1520 (1977).
[10]A. Omont, J. Phys. (Paris) **26**, 26 (1965).
[11]M. Chenevier, J. Dufayard, and J. C. Pebay-Peyroula, Phys. Lett. **25A**, 283 (1976).
[12]M. D. Havey, L. C. Balling, and J. J. Wright, J. Opt. Soc. Am. **67**, 488 (1977).
[13]H. Z. Kostlin, Z. Phys. **178**, 200 (1964).
[14]P. Hafner and W. H. E. Schwarz, J. Phys. B **11**, 2975 (1978).
[15]G. J. Victor (private communication), results obtained using the formalism of G. J. Victor, R. F. Stuart, and J. C. Laughlin, *Beam Foil Spectroscopy*, edited by J. Sellin and D. Pegg (Plenum, New York, 1976), Vol. 1, p. 43.